A GATE evaluation of the sources of error in quantitative ^{90}Y PET

Jared Strydhorst[a)]
*IMIV, U1023 Inserm/CEA/Université Paris-Sud and ERL 9218 CNRS, Université Paris-Saclay, CEA/SHFJ,
Orsay 91401, France*

Thomas Carlier
*Department of Nuclear Medicine, Centre Hospitalier Universitaire de Nantes and CRCNA, Inserm U892,
Nantes 44000, France*

Arnaud Dieudonné
Department of Nuclear Medicine, Hôpital Beaujon, HUPNVS, APHP and Inserm U1149, Clichy 92110, France

Maurizio Conti
Siemens Healthcare Molecular Imaging, Knoxville, Tennessee, 37932

Irène Buvat
*IMIV, U1023 Inserm/CEA/Université Paris-Sud and ERL 9218 CNRS, Université Paris-Saclay, CEA/SHFJ,
Orsay 91401, France*

Purpose: Accurate reconstruction of the dose delivered by ^{90}Y microspheres using a postembolization PET scan would permit the establishment of more accurate dose–response relationships for treatment of hepatocellular carcinoma with ^{90}Y. However, the quality of the PET data obtained is compromised by several factors, including poor count statistics and a very high random fraction. This work uses Monte Carlo simulations to investigate what impact factors other than low count statistics have on the quantification of ^{90}Y PET.

Methods: PET acquisitions of two phantoms—a NEMA PET phantom and the NEMA IEC PET body phantom-containing either ^{90}Y or ^{18}F were simulated using GATE. Simulated projections were created with subsets of the simulation data allowing the contributions of random, scatter, and LSO background to be independently evaluated. The simulated projections were reconstructed using the commercial software for the simulated scanner, and the quantitative accuracy of the reconstruction and the contrast recovery of the reconstructed images were evaluated.

Results: The quantitative accuracy of the ^{90}Y reconstructions were not strongly influenced by the high random fraction present in the projection data, and the activity concentration was recovered to within 5% of the known value. The contrast recovery measured for simulated ^{90}Y data was slightly poorer than that for simulated ^{18}F data with similar count statistics. However, the degradation was not strongly linked to any particular factor. Using a more restricted energy range to reduce the random fraction in the projections had no significant effect.

Conclusions: Simulations of ^{90}Y PET confirm that quantitative ^{90}Y is achievable with the same approach as that used for ^{18}F, and that there is likely very little margin for improvement by attempting to model aspects unique to ^{90}Y, such as the much higher random fraction or the presence of bremsstrahlung in the singles data. © *2016 American Association of Physicists in Medicine.*
[http://dx.doi.org/10.1118/1.4961747]

Key words: PET/CT simulation, GATE, yttrium-90, quantification

1. INTRODUCTION

The dosimetry of selective internal radiation therapy (SIRT) with ^{90}Y-microspheres is an important tool for balancing the efficacy and toxicity of radiation. In SIRT, radioactive spheres are injected via the hepatic arteries into the tumor where they become trapped in the capillary bed, irradiating the tumor. The treatment is typically simulated beforehand with ^{99}Tc-labeled macroaggregated albumin (MAA) and the distribution is observed using SPECT.[1–3] Several studies have correlated the dosimetry estimated from this pretreatment ^{99m}Tc MAA SPECT study to clinical outcome[4–6] with encouraging results.

However, it is likely that a direct post-treatment assessment of the actual ^{90}Y-microsphere distribution might provide more accurate dosimetry and better predict clinical outcome. Historically, such post-treatment study has been done using SPECT to detect and map the bremsstrahlung radiation generated by the ^{90}Y decay.[7–9] ^{90}Y SPECT however suffers from several deficiencies, including relatively low spatial resolution and the inherent challenges of quantitative SPECT.

PET can also be used to detect and map the distribution of ^{90}Y microspheres. This is possible because of a rare decay mode of ^{90}Y that produces positrons when the daughter isotope transitions to the ground state by internal pair production.

Several authors have already demonstrated the feasibility of using PET to obtain images of the 3D spatial distribution of ^{90}Y microspheres and have shown that the total activity recovered by using PET to detect ^{90}Y scales linearly with ^{90}Y activity.[10–16]

As part of this effort, this work aims to characterize the factors that limit the accuracy of ^{90}Y PET quantification and propose future steps toward overcoming these obstacles. Indeed, quantitative ^{90}Y PET encounters three potential difficulties:

1. Imaging with low true count statistics. ^{90}Y decays by β^- emission, almost exclusively to the ground state of ^{90}Zr (99.983%). A rare decay to the first excited state of ^{90}Zr occurs with a frequency of about 0.017%. One branch of the transition to the ground state is by internal pair production, resulting in on average 31.86 positrons for every 1×10^6 ^{90}Y decays.[17] PET images are typically reconstructed using iterative algorithms. Though unbiased in the high-count, high-iteration limit, with lower count statistics ordinary maximum likelihood algorithms are known to exhibit positive bias in regions of low activity.[18] Modified versions of the maximum likelihood (ML) reconstruction algorithms designed to reduce the bias in low-activity regions may therefore be useful for ^{90}Y PET.[19] These would include, for example, ABML, which imposes lower and upper boundaries (*A* and *B*) on the reconstructed values and allows for negative values in the reconstruction, or NEGML, which also permits negative values.

2. The broad spectrum of bremsstrahlung background extending into the PET energy window. The dominant effect is an increase in the number of random events in the projection data.

3. The comparatively large number of events due to the decay of ^{176}Lu in the LSO crystals of most modern PET scanners. This is not a significant problem with conventional PET tracers where the number of events from ^{176}Lu decay is very small relative to those from the tracer itself. However, when imaging ^{90}Y, this background accounts for the majority of the prompt events. The primary effect of ^{176}Lu is additional random counts in the projection data, although it is also possible for a gamma from the decay to be detected in coincidence with the energy deposited in the scintillation crystal by the beta emission from the same decay. Since they are correlated events, such LSO "trues" are not accounted for and corrected by the delayed counts.

Some groups have reported that the contrast recovery of ^{90}Y is poorer than for ^{18}F (Refs. 11, 14–16, and 20) using a PET image quality phantom.

The absolute accuracy of ^{90}Y PET is currently unclear, specifically whether accurate quantification can be achieved using system sensitivities measured for ^{18}F and making the necessary adjustments for branching ratio and half-life. Some of the difficulties in validating absolute calibration of ^{90}Y stem from the difficulty of directly and accurately measuring the activity of an almost pure beta emitter. Attarwala *et al.*[13] suggest that the system sensitivity for ^{90}Y is about 32% below that for ^{18}F. According to Carlier *et al.*,[14] the total activity in the FOV agreed with the activity in the scanner, though for a region of interest (ROI) containing only the hot region of the phantom they reported only 75%–80% of the true concentration. On the other hand, the QUEST study suggests that the uncertainty of absolute activity recovery is ±10%, though the error is sensitive to the choice of reconstruction parameters, particularly with lower activity levels.[16]

To date, the published research regarding ^{90}Y PET has used scan configurations and reconstruction algorithms developed and optimized for more conventional tracers, mostly labeled with ^{18}F. The purpose of this work is to investigate the differences between conventional PET and ^{90}Y PET, in particular the effects of the LSO background, of the bremsstrahlung background, and of the positron kinetic energy on the quantification of ^{90}Y PET. Monte Carlo simulations using GATE were used to quantify the influence of each effect. We simulated the PET data for two standard phantoms-the NEMA PET phantom (NU2-1994) and the NEMA IEC PET Body phantom (NU2-2001), and reconstructed the simulated data using the commercial software associated with the simulated PET scanner.

In this paper, the simulation of the NEMA PET 1994 phantom is presented and the relative contributions to the recorded coincidences from true events and from randoms arising from the bremsstrahlung and the LSO background were quantified. Images reconstructed from simulated projection data were quantified using the ^{18}F simulation as a reference for absolute activity quantification, and the effect of including or excluding the counts other than true unscattered events was evaluated. Finally, using the simulations of the IEC PET body phantom (2001), the influence of the random and scatter counts on the contrast ratios of hot and cold spheres was characterized. The simulated data were also compared to experimental data for the NEMA PET 1994 and the IEC PET body phantom.

2. METHOD

All simulations were performed with GATE v7.1 and GEANT4 v10.2beta, with the addition of a ^{90}Y bremsstrahlung model described below.

2.A. Scanner model

A GATE (Refs. 21 and 22) model of the PET portion of the Biograph mCT scanner was created, the significant parameters of which are summarized in Table I. The background activity from the decay of the ^{176}Lu in the crystals of the scanner was modeled using a generic ion source ($Z = 71$, $A = 176$, kinetic energy = 0) with a total activity of 3.30 MBq over all crystals. This activity was chosen such that the count rate for a simulation of an empty scanner agreed with that measured with our clinical Biograph PET-CT scanner. In the GATE digitizer, the crystal energy resolution was set to 11.7% at 511 keV with a quantum efficiency of 0.8. The pileup time was

TABLE I. Parameters of the GATE model of the Siemens Biograph mCT scanner.

Crystal material	LSO
Crystal size	$4 \times 4 \times 20$ mm
Ring diameter	842 mm
Crystals/ring	624
Rings	52
LSO activity	3.30 MBq
Energy resolution	11.7% @ 511 keV
Quantum efficiency	0.8
Pileup time	120 ns
Dead time	640 ns
Coincidence window width	4.1 ns
Delay window shift	500 ns
Energy window	435–650 keV

set to 120 ns. Singles, coincidences, and delays were recorded and stored in a ROOT output file. The coincidence window width was 4.1 ns, and the time shift for the delay window was 500 ns. Lower and upper energy thresholds were 435 and 650 keV, respectively, following the default settings for the Biograph scanner.[23] The image quality phantom simulations were also reconstructed using only events within a narrower energy window of 460–560 keV. Gaussian blurring with a FWHM of 2 mm was applied to the location of each detected event to simulate the positioning uncertainty of the block detector.

2.B. Simulated phantoms

The phantom simulations were set up to match as closely as possible previously acquired experimental data using two different phantoms.

Firstly, the cylindrical NEMA PET 1994 phantom (length: 200 mm, radius: 100 mm) was modeled as a cylinder of water. The source corresponding to the activity in one of the inserts was simulated as a cylinder (length: 180 mm, radius: 22.5 mm, 61.0 mm radially off center) within the larger cylinder.

To evaluate the singles contributions and the various event combinations contributing to the coincidence events, the cylindrical phantom was simulated with ^{90}Y activities of 30, 70, 150, 300, 700, 1500, and 3256 MBq in the insert. Simulations of 10 s were run using the GEANT4 general ion source to model the ^{90}Y.

An absolute calibration for converting reconstructed counts to activity was obtained from a 10-min simulation of the cylindrical phantom containing 1.5 MBq of ^{18}F. To evaluate the quantitative accuracy of activity concentration measured from reconstructed ^{90}Y images, a 60-min PET acquisition of the phantom containing 3256 MBq of activity was simulated using the fast ^{90}Y bremsstrahlung model described below.

Secondly, an IEC PET body phantom containing six spheres with diameters of 10, 13, 17, 22, 28, and 37 mm was created. Because the fast ^{90}Y bremsstrahlung model is only valid inside a scattering medium, the dimensions of the water phantom were padded by 6 mm all around, with the source activity confined to the dimensions of the actual phantom.

According to the simulations used to create the fast ^{90}Y model, about 98% of bremsstrahlung photons are produced within 6 mm of the source of the beta particles.

The image quality phantom contained a total activity of 3267 MBq (0.3 MBq/ml in the background) and a contrast ratio of 8:1, resulting in activity concentrations in the same order of magnitude as that observed in clinical practice. A second simulation was also conducted removing the activity from the spheres while maintaining the same activity concentration in the background for a total activity of 3152 MBq. The acquisition duration simulated for both phantoms was 30 min, typical of the duration used in clinical imaging.

The image quality phantom was also simulated with 5.3 kBq/ml of ^{18}F in the background and 42.4 MBq/ml in the spheres for a total of 57.7 MBq in the hot sphere phantom, and 55.7 MBq in the background of the cold sphere phantom.

For both the hot and cold sphere versions of the image quality phantom, the simulation was also run with just the ^{90}Y positron (i.e., with a positron with the same kinetic energy as the ^{90}Y positron, but no bremsstrahlung) to investigate the influence of positron range on contrast ratio.

2.C. Physics modelling

Two approaches were used to simulate the bremsstrahlung contribution from the decay of ^{90}Y. To measure the relative contributions from trues, scatter, and randoms generated by the source and by the LSO to the singles and coincidence rates, the ^{90}Y was modeled as an ion source ($Z = 39$, $A = 90$, kinetic energy = 0). The ion model does not include the internal pair production branch, which was modeled by adding a positron source.

For the longer acquisitions where reconstructed data were analyzed, complete modeling of the electron transport and bremsstrahlung production starting from an ion source is prohibitively slow, so a faster model was implemented. Following the approach described by Ref. 24, the energy spectrum and spatial and angular distribution of the primary bremsstrahlung produced by ^{90}Y were precalculated by a GATE simulation of a point source at the center of a sphere of water with a radius of 100 mm. A fast ^{90}Y model was then created for GATE to generate the primary bremsstrahlung photons directly in the region around the source, based on these distributions. The model included all bremsstrahlung photons produced up to 12 mm from the source, with energies up to 2 MeV. The internal pair-production branch of the ^{90}Y decay was modeled as a positron source with kinetic energies uniformly distributed between 0 and 738 keV.

All GATE simulations were run with the GEANT4 emstandard_opt3 physics list and the RadioactiveDecay process enabled.

2.D. Image reconstruction

The ROOT files generated by GATE were processed to create sinograms (400 pixels $\times$ 168 projection angles $\times$ 621 planes $\times$ 13 TOF bins) from the recorded coincidences, selected as follows:

(i) Trues: coincidences where both photons were produced by the same annihilation event from a ^{90}Y positron and neither has been scattered.

(ii) Trues+scatter: coincidences where both photons were produced by the annihilation of the same ^{90}Y positron, whether scattered or not.

(iii) Trues + ^{90}Y randoms: all trues (i) and all coincidences where the photons originated from different events, at least one of which involved ^{90}Y (positron annihilation or bremsstrahlung). Since the beta particle can have an energy as high as 2.28 MeV, it is also possible, though extremely unlikely, for two bremsstrahlung photons within the accepted energy window to be produced from a single event, creating a bremsstrahlung true.

(iv) Trues + ^{90}Y randoms + scatter: all coincidence events where at least one photon originated from the ^{90}Y (positron or bremsstrahlung).

(v) Trues + LSO randoms: all trues (i) plus random coincidences where both events originated from ^{176}Lu decay, either the energy deposited by the beta emission or one of the photons emitted by the de-excitation of the ^{176}Hf daughter. This includes LSO trues where both particles from the same decay are detected in coincidence.

(vi) All coincidence events.

The various sinograms were reconstructed using the commercial e7 reconstruction tools (version VG50) provided by Siemens. All data were reconstructed using an OS-EM reconstruction algorithm with two iterations and 21 subsets and time-of-flight (TOF). The reconstructed images were $400 \times 400 \times 109$ voxels with voxel dimensions of $2.036 \times 2.036 \times 2.072$ mm. The default point spread function model was enabled (axial direction: Gaussian, $\sigma = 1.9$ mm, radial PSF is a non-stationary function, see Ref. 25). Scatter correction was enabled for reconstructing data sets containing scattered events (ii, iv, vi). For quantitative analysis, no filtering was applied during or after the reconstruction.

The attenuation map provided to the reconstruction software was digitally created to match the geometry of the phantom modeled in GATE. The normalization sinograms required for the reconstruction were generated using GATE following the procedure described by Pépin *et al.*[26]

2.E. Phantom experiments

Scans of both the cylindrical and image quality phantom containing ^{90}Y were previously acquired with a Siemens Biograph mCT scanner. The cylindrical NEMA PET 1994 phantom contained 3.256 GBq of activity in one compartment at the time of the scan and no activity in the rest of the phantom. A 60-min scan was acquired. The IEC PET body phantom was acquired with a total of 3785 MBq of activity and an activity ratio of 8:1 in the spheres relative to the background. A full description of the acquisition protocols for both phantoms is included in Ref. 14. No experimental ^{18}F data were acquired.

2.F. Data analysis

The output of the ^{90}Y PET scans simulated with GATE was analyzed to determine the relative contributions of annihilation photons, bremsstrahlung photons, and events from the decay of ^{176}Lu in the detectors to the detected rates of single and coincidence events.

Reconstructed images of the simulated ^{18}F and ^{90}Y phantoms were analyzed using MATLAB to calculate the activity in the insert and cold regions of the phantom. The ROI for the insert was a cylinder slightly larger (47 mm diameter) than the actual cylinder of activity (45 mm diameter). Absolute activity calibration was calculated from the reconstructed ^{18}F image using the known activity and total counts inside the insert ROI.

To estimate the uncertainty on the measurements of mean activity, the cylindrical phantom was divided into ten sections each with a thickness of 7 slices (14 mm) along the axial direction, with one slice skipped between each section. The values reported are the mean total activity and the standard error of the mean.

For the image quality phantom, the ^{18}F images were reconstructed with all counts, and with the number of net true counts reduced to match the counts available for the ^{90}Y reconstruction. Ten low count ^{18}F simulations were reconstructed to provide an estimate of the uncertainty of the contrast recovery coefficient (CRC) obtained when reconstructing data with poor count statistics typical of ^{90}Y. Ten ^{90}Y images were also reconstructed using all the prompt counts. The contrast recovery coefficients for both isotopes were calculated following the procedure specified by the NEMA NU 2–2001 standard.[27] ROIs for the hot spheres were created with the true diameter and position of each sphere. For the background, 12 circular ROIs were created in each of the central plane and the planes ±10 and ±20 mm away for a total of 60 background ROIs. The CRC for the hot sphere phantom was calculated as

$$\mathrm{CRC}_{\mathrm{hot}} = \frac{C_{\mathrm{hot}}/C_{\mathrm{bkg}} - 1}{A_{\mathrm{hot}}/A_{\mathrm{bkg}} - 1}.$$

C_{hot} and C_{bkg} are the mean activity concentration recovered in the hot sphere and background ROIs respectively, and A_{hot} and A_{bkg} are the true activity concentrations.

For the cold sphere analysis, the CRC was calculated as follows:

$$\mathrm{CRC}_{\mathrm{cold}} = 1 - \left(C_{\mathrm{cold}}/C_{\mathrm{bkg}} \right).$$

The background variability is reported as the coefficient of variation of C_{bkg} for the 37 mm ROIs,

$$\text{background variability} = \frac{\sigma_{C_{\mathrm{bkg}}}}{\overline{C_{\mathrm{bkg}}}}.$$

3. RESULTS

3.A. Singles rates

For the NEMA94 phantom, the simulated singles rate of unscattered photons from positron annihilation in the
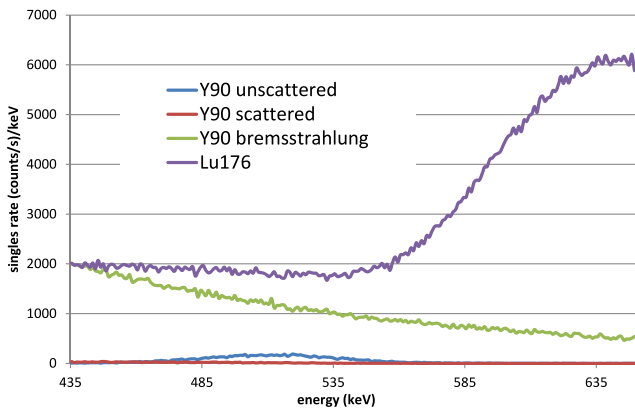
FIG. 1. Relative contribution to the singles from the scattered and unscattered annihilation photons, bremsstrahlung, and decay of ^{176}Lu, with 3.256 GBq of ^{90}Y activity in the NEMA94 phantom.

435–650 keV energy window was 3.435 ± 0.008 (cts/s)/MBq. For scattered photons, the singles rate was 0.6054 ± 0.0003 (cts/s)/MBq, and for bremsstrahlung photons, it was 69.6 ± 0.5 (cts/s)/MBq. The singles rate increased linearly with the activity of the ^{90}Y. The background rate of singles from decay of the ^{176}Lu in the LSO crystals was $641\,500 \pm 100$ cts/s independent of the phantom activity.

The singles rates from positron annihilation, from bremsstrahlung photons and from ^{176}Lu decays are shown in Fig. 1.

3.B. Prompts and delayed activity

The relative contribution to the prompt coincidences from the various physical events as a function of the ^{90}Y activity is shown in Fig. 2.

The rate of true coincidences of only unscattered photons from ^{90}Y was 0.174 (cts/s)/MBq. The rate of coincidences where at least one of the photons was scattered in the phantom was 0.0657 (cts/s)/MBq. Both rates increased linearly with the ^{90}Y activity.

The rate of random coincidence events in which at least one photon originated from the ^{90}Y was 0.279 (cts/s)/MBq.

Random coincidences where both events originated from the decay of ^{176}Lu accounted for a constant background of

1182 cts/s. An additional background from LSO trues is also present, contributing about 5.4 cts/s with no other activity in the scanner. The number of LSO true events increased slightly with the amount of ^{90}Y in the scanner, contributing about 27 cts/s with 3.256 GBq of ^{90}Y activity. Finally, a very small number of bremsstrahlung true events was also detected: $(1.38 \pm 0.14) \times 10^{-5}$ (cts/s)/MBq.

3.C. Comparison of simulated and experimental data

The 60 min experimental acquisition of the cylindrical ^{90}Y NEMA phantom resulted in 10.8×10^{6} prompts and 7.71×10^{6} delayed counts [random fraction (RF): 71.3%]. The simulation of the same experimental setup resulted in 10.3×10^{6} prompts and 7.42×10^{6} delayed counts (RF: 71.7%).

3.D. Absolute activity

Figure 3 shows the total reconstructed ^{90}Y activity contained within the insert and Fig. 4 shows the percentage of the activity measured in the phantom but outside the insert using the NEMA94 PET phantom.

Including or not including the scattered, randoms, and LSO counts in the projections had a very limited effect on the activity measured in the insert. With only true counts in the projections, the measured activity was 0.9% above the true

FIG. 3. Activity concentration in the insert of the ^{90}Y phantom. Error bars show the standard error of the mean. The true activity concentration in the insert is indicated by the red line.
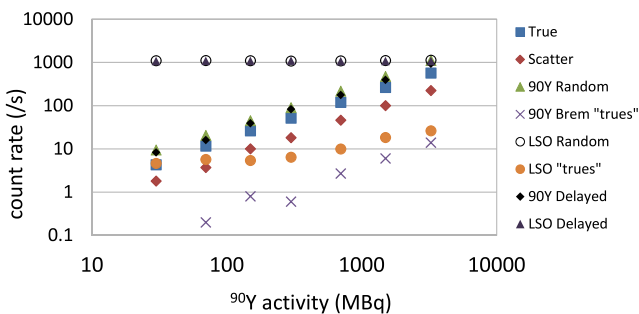

FIG. 2. Contributions of true, scattered, and random counts from the ^{90}Y and the LSO to total prompt counts recorded. True, scattered, and random events all refer to events in the prompt coincidence window, sorted using the sourceID, eventID, and comptonPhantom tags in GATE. The delayed events refer to events detected in the delayed coincidence window.
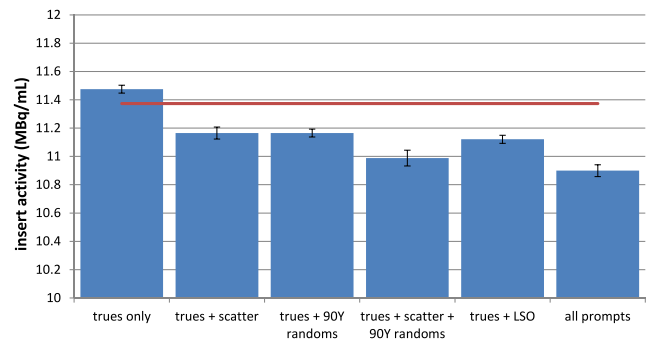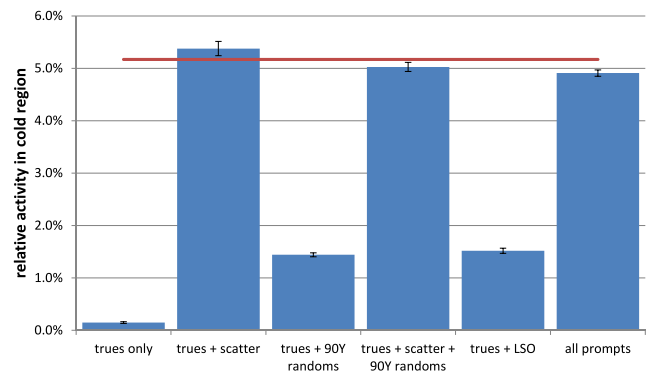

FIG. 4. Activity in the cold region of the ^{90}Y phantom as a percentage of the activity in the hot region. Error bars show the standard error of the mean. The activity measured for the ^{18}F simulations is indicated by the red line.
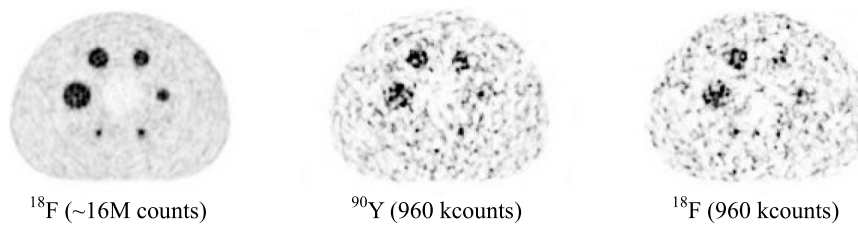
FIG. 5. Cross sections of reconstructed simulations of the image quality phantom.

activity and 2%–4% below the true activity when the other events-scatter, bremsstrahlung, and background LSO decay-were included.

The bremsstrahlung, random, and scattered counts did influence the activity measured in the cold background, but the absolute magnitude of the effect was small. Scatter accounted for the largest effect, resulting in a total background activity of about 5% of that in the hot region, the same as observed with ^{18}F. The effect of the random events from either bremsstrahlung or LSO decay on the background activity was only about 1.5% when considered separately, and had essentially no additional quantitative influence when scatter was also present.

3.E. Contrast ratio

Figure 5 shows the central slice of the reconstructed hot sphere phantom for ^{18}F data, ^{90}Y data, and ^{18}F data with the same number of net true counts as the ^{90}Y data. In the low count images, only the three largest spheres can be visually distinguished from noise.

The hot sphere CRCs for the simulations of the image quality phantom and an actual ^{90}Y phantom acquisition are shown in Fig. 6. The CRC of the ^{18}F was slightly better than that for the ^{90}Y in most cases, though not significantly so. The simulated ^{90}Y data exhibited better contrast recovery than the experimental data.
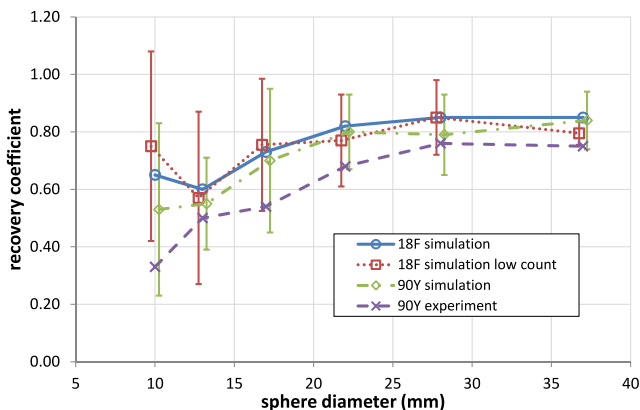
Figure 7 shows the hot sphere CRC for one phantom reconstructed with different subsets of the ^{90}Y data: true counts only, true counts with scatter, with bremsstrahlung randoms, with LSO randoms, and with all of the counts present.

Figure 8 shows the cold sphere CRC for ^{18}F (all counts), ^{18}F with a restricted number of counts, and ^{90}Y. The mean CRCs of the low count ^{18}F data were comparable to those for the high-count ^{18}F data. The CRC of the ^{90}Y simulations was consistently poorer than that of ^{18}F images with similar count statistics. The cold sphere CRCs for the ^{90}Y images with various subsets of the count data are shown in Fig. 9.

The background variability of the ^{18}F images was 5.1% and 20.3% for the normal and low-count data, respectively. The background variability of the ^{90}Y images was 24.8%.

The recovery coefficients for the ^{90}Y hot- and cold-sphere phantoms using the default (435–650 keV) energy window and a more restricted 460–560 keV energy window are shown in Fig. 10.

Comparison of the ^{18}F hot- and cold-sphere phantom simulations with the ^{90}Y positron-only simulations is shown in Fig. 11.

4. DISCUSSION

4.A. Singles and coincidences

The most apparent difference between ^{90}Y PET data and ^{18}F PET data is the relatively high random fraction. Even with over 3 GBq of ^{90}Y activity in the cylindrical phantom, positron annihilation accounts for less than 2% of the singles detected

FIG. 6. Contrast recovery coefficients for a simulation with ^{18}F ($\sim 23 \times 10^6$ net counts), the experimental ^{90}Y acquisition (1.36×10^6 net counts), ^{18}F with 1.01×10^6 net counts, and ^{90}Y (1.01×10^6 net counts). The error bars are the standard deviation of the CRC achieved over ten different simulations of the low count simulations.
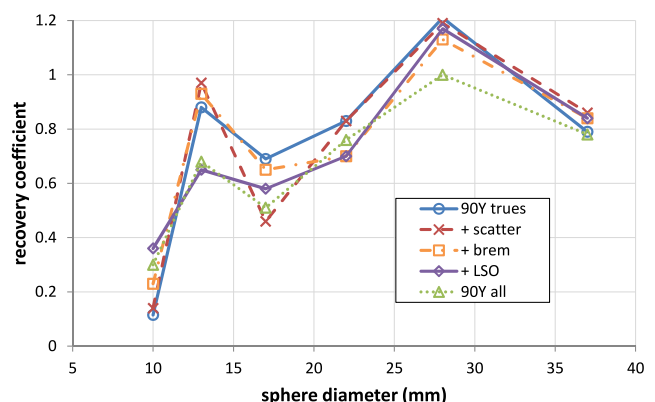

FIG. 7. Contrast recovery coefficients of the hot spheres with images reconstructed from subsets of the simulated counts: trues only, trues + scatter, trues + bremsstrahlung, trues + LSO background (randoms + trues), and all counts.
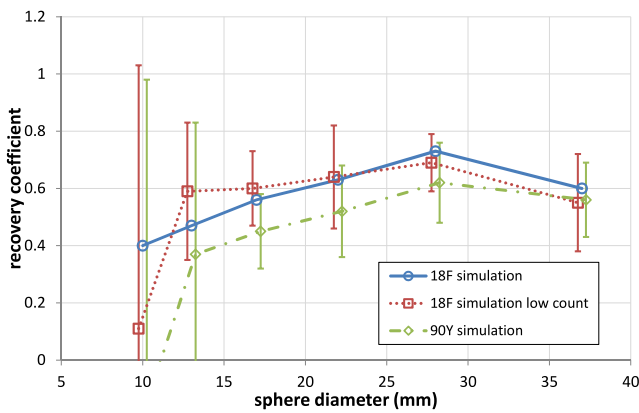
FIG. 8. Contrast recovery coefficients for the cold sphere phantom for ^{18}F, ^{90}Y, and low count ^{18}F. The error bars are the standard deviations of 10 noise realizations.

of which about 20% have been scattered in the phantom. Bremsstrahlung from the beta emission of ^{90}Y contributes about 15–20 singles for every true single registered. The vast majority of the singles, at least 70%, come from the Lu decay and bremsstrahlung. By comparison, for the same phantom containing 370 MBq of ^{18}F, only about 1.5% of the singles come from the decay of ^{176}Lu.

Of the coincidences detected with 3.256 GBq of ^{90}Y, less than 20% are true coincidences produced by positrons from the ^{90}Y decay, about 7% are from annihilation events where at least one of the photons has scattered in the phantom before reaching the detector, with the rest made up of random coincidences, approximately half of which come entirely from the background decay of the ^{176}Lu.

The rate of bremsstrahlung true events is nearly two orders below the rate of genuine coincidence events and is unlikely to influence quantification. The rate of LSO trues is also well below the rate of genuine trues, except for very low source activities. However, with TOF reconstruction, the contribution from these events should be relegated to the margins of the reconstruction. It is unexpected to see the rate of LSO trues
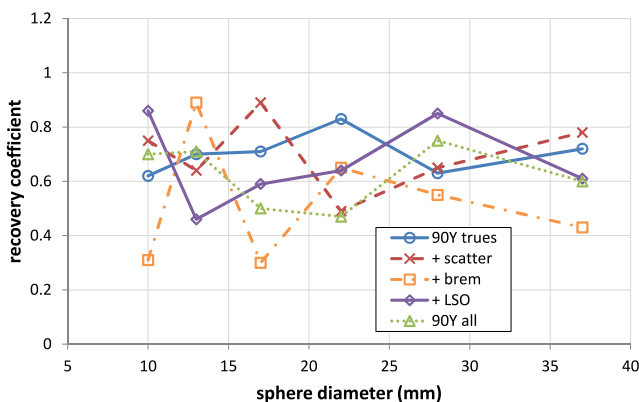
increasing with the ^{90}Y activity, since this should be a constant background. We suspect this is an artifact of the way events are labeled in GATE: when a single event is created by summing the energy from more than one particle deposited in the same block within an integration period, the eventID label of only one of the contributing particles will be assigned to the single pulse event that results. Possibly, by combining with energy deposited by a bremsstrahlung photon, a 307 or 202 keV photon emitted by LSO decay is more likely to produce a pulse in the accepted energy window.

4.B. Randoms and scatter

The randoms, whether from the bremsstrahlung or the ^{176}Lu decay or a combination of both, are accounted for by the delayed coincidence window. However, despite the high random fraction, we detected no significant influence on the quantification of ^{90}Y that could be attributed to the presence of random events. Reconstructing only true events, true and random events, and all events resulted in virtually identical results for absolute quantification (Fig. 3). This seems consistent with other studies reporting generally accurate quantification despite the high random fraction in ^{90}Y data.[14]

In approximately 7.6% of the coincidences recorded, one or both of the photons had been scattered, accounting for about 22% of the net trues. Scatter had only a very small effect on the quantification of the hot regions, reducing the activity concentration by about 4%. The impact of scatter on the activity measured in the cold region of the phantom was larger, resulting in a total activity in the cold region about 5% of that in the hot region, compared to 0.2% for reconstruction where the scattered events had been removed (Fig. 4). The influence of scatter on quantification in the cold region seems to be exactly the same as that observed in ^{18}F imaging.

4.C. Absolute quantification

Overall, the only error in absolute quantification of the ^{90}Y using a calibration obtained using ^{18}F was a very small underestimate of the ^{90}Y activity of approximately 4% (Fig. 3). This may be the result of a small reduction in scanner sensitivity because of pileup involving bremsstrahlung photons, although the GATE digitizer may not reproduce the behavior of a real scanner precisely enough to have a great deal of confidence in the simulations at this level of detail. Further investigation of the detector response to ^{90}Y may be worthwhile, but would require a detailed description of the detector hardware and front-end electronics, which will depend on the manufacturer and model of the scanner. Since the models, simulation, and processing were identical, this small discrepancy likely has some basis in the differences between ^{18}F and ^{90}Y (possibly the presence of the bremsstrahlung affects the detector or shifts the energy of some of the detected pulses). Moreover, the activity measured in the cold region of the phantom was nearly identical for both ^{90}Y and ^{18}F. These results differ from the significantly lower system sensitivity for ^{90}Y (-32%) reported by Ref. 13, and that from Ref. 14, where the activity in the insert was measured to be about 20% below the true activity.

FIG. 9. Contrast recovery coefficients of the cold spheres with images reconstructed from subsets of the simulated counts: trues only, trues + scatter, trues + bremsstrahlung, trues + LSO background (randoms + trues), and all counts.
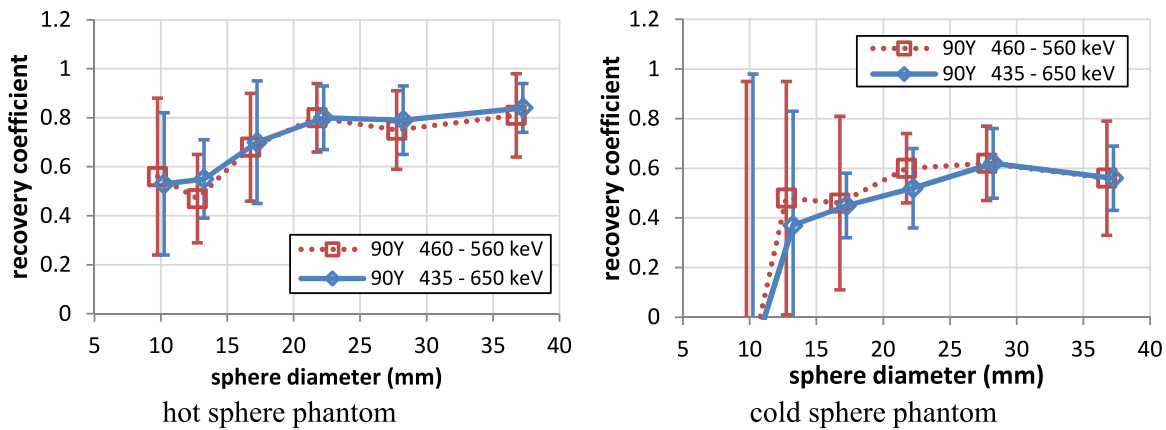
FIG. 10. Recovery coefficients obtained using the default energy window and a more restricted energy window.

Some of this discrepancy could arise from the uncertainty in accurately measuring the activity of a sample of ^{90}Y, and we observed nothing that could explain a discrepancy as large as 30%. However, this agrees well with the results reported by Ref. 16, which showed that for the Siemens Biograph mCT and GE Discovery scanners the quantification was generally accurate to better than 10% for large regions, with perhaps a slight negative bias for most of the tested combinations of reconstruction parameters.

4.D. Contrast recovery

For the contrast recovery measured with the image quality phantom, only minor differences between ^{90}Y and ^{18}F were detectable for projection data with similar numbers of net counts. For the simulated data, the CRCs measured for the hot spheres were virtually identical for ^{18}F and ^{90}Y (Fig. 6). The experimental CRCs for the ^{90}Y were consistently lower than those obtained from the ^{90}Y simulations, suggesting either that there is still some factor limiting contrast recovery not fully accounted for in the GATE model, or that the true contrast ratio in the experimental setup was slightly less than 8:1.
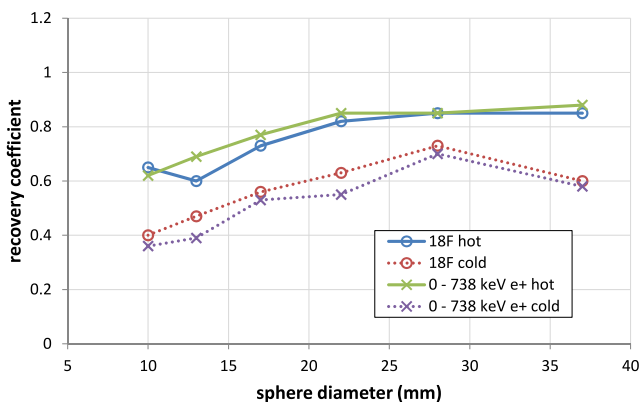

FIG. 11. Contrast recovery coefficients for simulations of the IEC PET body phantom containing ^{18}F and the ^{90}Y positron alone with ^{18}F-like count statistics (~12×10^6 net trues).

For the cold spheres, the contrast recovery was consistently lower for the ^{90}Y than for the ^{18}F (Fig. 8). This may be partly related to the higher average positron kinetic energy of ^{90}Y relative to ^{18}F. Figure 11 compares the contrast recovery between ^{18}F and a positron source with a ^{90}Y-like kinetic energy, both with high count statistics, and does imply a small degradation in cold sphere contrast ratio as a result of the high positron range. For the hot spheres, the more energetic positron unexpectedly resulted in marginally better contrast recovery.

Comparing the contrast recovery for different subsets of the ^{90}Y count data revealed no clearly dominant contribution from any of the scatter, random, or LSO background contributions: although including or excluding the counts from each in the reconstruction did change the measured contrast ratio, the changes exhibited no consistent pattern across the range of sphere sizes (Fig. 7). For the hot spheres, the trues-only reconstructions generally outperformed the reconstructions with all counts, and the reconstruction with trues and LSO background seems to be the most consistent outlier, but it is difficult to draw any firm conclusions given the amount of noise in the data. The data for the cold sphere phantom (Fig. 9) exhibit no clear pattern at all suggesting that any one effect might dominate.

Limiting the coincidence photons to the range 460–560 keV removes a large portion of the LSO background and some of the lower energy bremsstrahlung photons. However, this did not result in any appreciable difference in the contrast recovery (Fig. 10). This is somewhat surprising, since narrowing the window does substantially reduce the random fraction, from about 75% to approximately 35% for the IEC PET body phantom. It is however consistent with the observation that images reconstructed with trues-only did not exhibit consistently better contrast recovery than those with randoms included (Figs. 7 and 9). It may also be that the low count statistics are the dominant factor limiting the contrast recovery, overshadowing any improvement derived from a lower random fraction.

Overall, our results imply that the relatively high random fraction of ^{90}Y imaging is effectively handled by the random correction algorithm, since removing the randoms from the projections had very little effect on the quantification of ^{90}Y and little systematic impact on the measured contrast ratios. This suggests that the benefits of using a BGO scanner to

reduce the background would be outweighed by the loss of the ability to do TOF reconstruction.

This work was done using standard PET phantoms. Although this made it possible to validate this simulated data using experimental data and it seems reasonable to expect that the quantitation and contrast measured in these phantoms would be similar to that in clinical situations, these phantoms do not provide the best simulation of the real distributions that occur in patients. Thus, it may be beneficial to confirm these results using more realistic models of activity distribution. Moreover, it would be interesting to quantify the influence of the parameters investigated on the calculated dosimetry.

5. CONCLUSIONS

The absolute quantification of ^{90}Y activity based on ^{18}F calibration exhibits a very small systematic offset compared to that obtained using ^{18}F activity at the same count rate as that measured using ^{90}Y. This offset is less than 5% for activity concentration similar to that used clinically in SIRT with ^{90}Y-microspheres, in agreement with the QUEST study, but considerably better than that previously reported by two other experimental studies. The scatter, ^{90}Y bremsstrahlung, and the LSO background all slightly degrade the observed contrast ratio, though none of the contributions appears to be dominant, and quantification seems unlikely to be improved by ^{90}Y-specific compensation in the reconstruction algorithm. Any further improvement in the quantitative accuracy of the reconstruction is likely to come from reconstruction methods optimized to address the poor count statistics, rather than better modeling the ^{90}Y specific behavior of the scanner.

CONFLICT OF INTEREST DISCLOSURE

The authors have no COI to report.

a)Author to whom correspondence should be addressed. Electronic mail: jared.strydhorst@gmail.com

[1]A. Kennedy, S. Nag, R. Salem, R. Murthy, A. J. McEwan, C. Nutting, B. I. Al, J. Espat, J. I. Bilbao, R. A. Sharma, J. P. Thomas, and D. Coldwell, "Recommendations for radioembolization of hepatic malignancies using yttrium-90 microsphere brachytherapy: A consensus panel report from the radioembolization brachytherapy oncology consortium," Int. J. Radiat. Oncol., Biol., Phys. **68**, 13–23 (2007).

[2]S. Ho, W. Y. Lau, T. W. Leung, M. Chan, Y. K. Ngar, P. J. Johnson, and A. K. Li, "Partition model for estimating radiation doses from yttrium-90 microspheres in treating hepatic tumours," Eur. J. Nucl. Med. **23**, 947–952 (1996).

[3]A. Dieudonné, E. Garin, S. Laffont, Y. Rolland, R. Lebtahi, D. Leguludec, and I. Gardin, "Clinical feasibility of fast 3-dimensional dosimetry of the liver for treatment planning of hepatocellular carcinoma with ^{90}Y-microspheres," J. Nucl. Med. **52**, 1930–1937 (2011).

[4]P. Flamen, B. Vanderlinden, P. Delatte, G. Ghanem, L. Ameye, and A. Hendlisz, "Multimodality imaging can predict the metabolic response of

[5]E. Garin, L. Lenoir, Y. Rolland, J. Edeline, H. Mesbah, S. Laffont, P. Poree, B. Clement, J.-L. Raoul, and E. Boucher, "Dosimetry based on ^{99m}Tc-macroaggregated albumin SPECT/CT accurately predicts tumor response and survival in hepatocellular carcinoma patients treated with ^{90}Y-loaded glass microspheres: Preliminary results," J. Nucl. Med. **53**, 255–263 (2012).

[6]C. Chiesa, M. Mira, M. Maccauro, C. Spreafico, R. Romito, C. Morosi, T. Camerini, M. Carrara, S. Pellizzari, A. Negri, G. Aliberti, C. Sposito, S. Bhoori, A. Facciorusso, E. Civelli, R. Lanocita, B. Padovano, M. Migliorisi, E. Seregni, A. Marchiano, F. Crippa, and V. Mazzaferro, "Radioembolization of hepatocarcinoma with ^{90}Y glass microspheres: Development of an individualized treatment planning strategy based on dosimetry and radiobiology," Eur. J. Nucl. Med. Mol. Imaging **42**, 1718–1738 (2015).

[7]M. Elschot, M. G. E. H. Lam, M. A. A. J. van den Bosch, M. A. Viergever, and H. W. A. M. de Jong, "Quantitative Monto Carlo-based ^{90}Y SPECT reconstruction," J. Nucl. Med. **54**, 1557–1563 (2013).

[8]X. Rong, Y. Du, M. Ljungberg, E. Rault, S. Vandenberghe, and E. C. Frey, "Development and evaluation of an improved quantitative ^{90}Y bremsstrahlung SPECT method," Med. Phys. **39**, 2346–2358 (2012).

[9]D. Minarik, G. K. Sjogreen, and M. Ljungberg, "Evaluation of quantitative ^{90}Y SPECT based on experimental phantom studies," Phys. Med. Biol. **53**, 5689–5703 (2008).

[10]R. Lhommel, L. van Elmbt, P. Goffette, M. Van den Eynde, F. Jamar, S. Pauwals, and S. Walrand, "Feasibility of ^{90}Y TOF PET-based dosimetry in liver metastasis therapy using SIR-Spheres," Eur. J. Nucl. Med. Mol. Imaging **37**, 1645–1662 (2010).

[11]K. Willowson, N. Forwood, B. W. Jakoby, A. M. Smith, and D. L. Bailey, "Quantitative ^{90}Y image reconstruction in PET," Med. Phys. **39**, 7153–7159 (2012).

[12]Y.-H. Kao, J. D. Steinberg, Y.-S. Tay, G. K. Lim, J. Yan, D. W. Townsend, C. A. Budgeon, J. A. Boucek, R. J. Francis, T. S. Cheo, M. C. Burgmans, F. G. Irani, R. H. Lo, K.-H. Tay, B.-S. Tan, P. K. Chow, S. Stachithanantham, A. E. Tan, D. C. Ng, and A. S. Goh, "Post-radioembolization yttrium-90 PET/CT. Part II. Dose response and tumor predictive dosimetry for resin microspheres," EJNMMI Res. **3**, 57, 1-12 (2013).

[13]A. A. Attarwala, F. Molina-Duran, K.-A. Büsing, S. O. Schönberg, D. L. Bailey, K. Willowson, and G. Glatting, "Quantitative and qualitative assessment of yttrium-90 PET/CT imaging," PLoS One **9**, e110401 (2014).

[14]T. Carlier, K. Willowson, E. Fourkal, D. L. Bailey, M. Doss, and M. Conti, "^{90}Y-PET imaging: Exploring limitations and accuracy under conditions of low counts and high random fractions," Med. Phys. **42**, 4295–4309 (2015).

[15]T. Carlier, T. Eugene, C. Bodet-Milin, E. Garin, C. Ansquer, C. Rousseau, L. Ferrer, J. Barbet, F. Schoenahl, and F. Kraeber-Bodere, "Assessment of acquisition protocols for routine imaging of ^{90}Y using PET/CT," EJNMMI Res. **3**, 11, 1-12 (2013).

[16]K. P. Willowson, M. Tapner, QUEST Investigator Team, and D. L. Bailey, "A multicentre comparison of quantitative ^{90}Y PET/CT for dosimetric purposes after radioembolization with resin microspheres: The QUEST phantom study," Eur. J. Nucl. Med. Mol. Imaging **42**, 1202–1222 (2015).

[17]R. G. Selwyn, R. J. Nickles, B. R. Thomadsen, L. A. DeWerd, and J. A. Micka, "A new internal pair production branching ratio of ^{90}Y: The development of a non-destructive assay for ^{90}Y and ^{90}Sr," Appl. Radiat. Isot. **65**, 318–327 (2007).

[18]K. Van Slambrouck, S. Stute, C. Comtat, M. Sibomana, F. H. P. van Velden, R. Boellaard, and J. Nuyts, "Bias reduction for low-statistics PET: Maximum likelihood reconstruction with a modified Poisson distribution," IEEE Trans. Med. Imaging **34**, 126–136 (2015).

[19]M. Conti, V. Panin, J. Hong, T. Carlier, and K. Parodi, "Monitoring hadron and ^{90}Y therapies: PET reconstruction at extremely low counts," in *IEEE Nuclear Science Symposium Conference Record* (2014).

[20]M. D'Arienzo, P. Chiaramida, L. Chiacchiararelli, A. Coniglio, R. Cianni, R. Salvatori, A. Ruzza, F. Scopinaro, and O. Bagni, "^{90}Y PET-based dosimetry after selective internal radiotherapy treatments," Nucl. Med. Commun. **33**, 633–640 (2012).

[21]S. Jan, G. Santin, D. Strul, S. Staelens, K. Assié, D. Autret, S. Avner, R. Barbier, and C. Morel, "GATE: A simulation toolkit for PET and SPECT," Phys. Med. Biol. **49**, 4543–4561 (2004).

[22]S. Jan, D. Benoit, E. Becheva, T. Carlier, F. Cassol, P. Descourt, T. Frisson, and I. Buvat, "GATE V6: A major enhancement of the GATE simulation platform enabling modeling of CT and radiotherapy," Phys. Med. Biol. **56**, 881–901 (2011).

[23]B. W. Jakoby, Y. Bercier, M. Conti, M. E. Casey, B. Bendriem, and D. W. Townsend, "Physical and clinical performance of the mCT time-of-flight PET/CT scanner," Phys. Med. Biol. **56**, 2375–2389 (2011).

[24]E. Rault, S. Staelens, R. Van Holen, J. De Beenhouwer, and S. Vandenberghe, "Fast simulation of yttrium-90 bremsstrahlung photons with GATE," Med. Phys. **37**, 2943–2950 (2010).

[25]V. Panin, F. Kehren, C. Michel, and M. Casey, "Fully 3-D PET reconstruction with system matrix derived from point source measurements," IEEE Trans. Med. Imaging **25**, 907–921 (2006).

[26]A. Pépin, S. Stute, S. Jan, and C. Comtat, "Normalization of Monte Carlo PET data using GATE," in *Nuclear Science Symposium and Medical Imaging Conference (NSS/MIC), 2011 IEEE* (IEEE, Piscataway, NJ, 2011), pp. 4196–4200.

[27]National Electronic Manufacturers Association, NEMA Standards Publication NU 2–2001: Performance Measurements of Positron Emission Tomographs, National Electronic Manufacturers Association, Rosslyn, VA, 2001.